DOI: 10.1002/chem.200500103

Sensitivity of Transmission Surface Plasmon Resonance (T-SPR) Spectroscopy: Self-Assembled Multilayers on Evaporated Gold Island Films

Ilanit Doron-Mor,[a] Hagai Cohen,[b] Zahava Barkay,[c] Abraham Shanzer,[d] Alexander Vaskevich,[a] and Israel Rubinstein*[a]

Abstract: The distance dependence of the localized surface plasmon (SP) extinction of discontinuous gold films is a crucial issue in the application of transmission surface plasmon resonance (T-SPR) spectroscopy to chemical and biological sensing. This derives from the usual sensing configuration, whereby an analyte binds to a selective receptor layer on the gold film at a certain distance from the metal surface. In the present work the distance sensitivity of T-SPR spectroscopy of 1.0–5.0 nm (nominal thickness) gold island films evaporated on silanized glass substrates is studied by using coordination-based self-assembled multilayers, offering thickness tuning in the range from ~1 to ~15 nm. The morphology, composition and optical properties of the Au/multilayer systems were studied at each step of multilayer construction. High-resolution scanning electron microscopy (HRSEM) showed no apparent change in the underlying Au islands, while atomic force microscopy (AFM) indicated flattening of the surface topography during multilayer construction. A regular growth mode of the organic layers was substantiated by X-ray photoelectron spectroscopy (XPS). Transmission UV-visible spectra showed an increase of the extinction and a red shift of the maximum of the SP band upon addition of organic layers, establishing the distance dependence of the Au SP absorbance. The distance sensitivity of T-SPR spectroscopy can be varied by using characteristic substrate parameters, that is, Au nominal thickness and annealing. In particular, effective sensitivity up to a distance of at least 15 nm is demonstrated with 5 nm annealed Au films. It is shown that intensity measurements, particularly in the plasmon intensity change (PIC) presentation, provide an alternative to the usually measured plasmon band position, offering good accuracy and the possibility of measuring at a single wavelength. The present distance sensitivity results provide the basis for further development of T-SPR transducers based on receptor-coated Au island films.

Keywords: gold · multilayers · self-assembly · sensors · surface plasmon resonance

Introduction

Transmission UV-visible spectra of Au and Ag island films, as well as those of structures comprised of metal nanoparticles, exhibit a characteristic absorption band attributed to excitation of localized surface plasmon (SP) polaritons. The conditions for SP resonance depend on the metal film morphology, that is, island size, shape, spatial organization, and the dielectric properties of the contacting medium.[1,2] The dependence of the SP absorption band (wavelength, intensity) of metal island films on the dielectric constant of bathing solvents is well established.[3–7] Recently we[8–10] and others[11] have demonstrated sensitivity of the SP band of Au and Ag island films to various adsorbed molecular layers. The method, termed transmission surface plasmon resonance (T-SPR) spectroscopy, offers a combination of high sensitivity and simple experimental requirements. T-SPR spectroscopy was shown to be applicable to both chemically and physically adsorbed molecules in liquid or gas phase.[8–10] The T-SPR approach is particularly promising for biosensing, and the first examples have been published recently.[12–19]

[a] I. Doron-Mor, Dr. A. Vaskevich, Prof. I. Rubinstein
Department of Materials and Interfaces
Weizmann Institute of Science, Rehovot 76100 (Israel)
Fax: (+972) 8-934-4137
E-mail: israel.rubinstein@weizmann.ac.il

[b] Dr. H. Cohen
Department of Chemical Research Support
Weizmann Institute of Science, Rehovot 76100 (Israel)

[c] Dr. Z. Barkay
Wolfson Materials Center, Tel-Aviv University
Tel-Aviv 69978 (Israel)

[d] Prof. A. Shanzer
Department of Organic Chemistry
Weizmann Institute of Science, Rehovot 76100 (Israel)

Application of T-SPR spectroscopy to actual sensing, and particularly to biosensing, involves construction of complex interfaces, promoting selective binding of desired analytes while preventing nonspecific binding. Systems of this kind would normally require a multilayer structure including selective receptors as well as blocking layers, all assembled on the metal island film. The target analyte molecules would therefore be bound to a receptor layer at a certain distance from the metal island surface. Consequently, the sensitivity and distance dependence of T-SPR response to analyte binding becomes a major issue in the design and optimization of sensing elements.

Studies of distance-dependent properties of evanescent waves in metal island films have been stimulated by the development of the electromagnetic theory of surface-enhanced Raman spectroscopy (SERS).[20,21] Several experimental approaches have been used to achieve controlled separation between the metal surface and probe molecules in SERS studies; that is, deposition of ultrathin polymeric films[22,23] or silica overcoats,[24–27] Langmuir–Blodgett multilayers,[28,29] and self-assembled monolayers (SAMs).[30,31] These methods provide a separation in the range of ~2–15 nm. The sensitivity of the localized SP of nanostructured metal films to changes in the effective dielectric constant of the contacting medium has been studied using similar approaches. Van Duyne, Schatz, and co-workers[11,32] studied the distance dependence of the SP absorbance of relatively large Ag and Au nanoparticle films (characteristic dimensions are an order-of-magnitude larger than the average island dimensions (diameter, height) in the Au island films investigated here.[33]) A silica shell was used by Liz-Marzan, Mulvaney, and co-workers in a study of the distance dependence of the SP band of Au nanoparticles (NPs) in solution and in a multilayer film.[34–36] Layer-by-layer assembly of a polyelectrolyte film on a Au NP monolayer was exploited by Schmitt et al. in a study of the distance dependence of the SP band.[37] This last group of authors mentioned that the local dielectric environment influences not only the position of the absorption band, but, even more drastically, the intensity of the SP absorbance.

Quantitative treatment of the localized SP absorption of nanostructured metal films is highly complex due to the interplay between interactions of the metal islands packed in a dense random array, and variations in the island shape.[38] Using a discrete dipole approximation, Schatz and co-workers qualitatively described the optical response of regular arrays of large pyramidal Ag islands.[39,40] An approach based on the mean-field Maxwell–Garnett approximation gives a semiquantitative agreement between theoretical prediction and experimental data for the shift in the wavelength of SP maximum, in the simplest case of monodisperse metal NP layers.[34–37,41]

In the present study the distance sensitivity of the T-SPR response of evaporated Au island films is evaluated by using coordination-based self-assembled multilayers, previously studied by us on continuous, evaporated Au substrates.[42–45] This approach is extended here to the layer-by-layer construction of similar multilayers on Au island films. The multilayers are prepared by coordination self-assembly, including binding of Zr^{IV} ions to a self-assembled monolayer of disulfide–bishydroxamate anchor molecules on the Au followed by alternate binding of layers of bifunctional tetrahydroxamate molecules and Zr^{IV} ions (Figure 1). The regular growth of the multilayer provides a tunable distance in the range from ~1 to ~15 nm, enabling us to study the distance dependence of the optical response of Au island films and affording an excellent simulation of actual T-SPR sensing.[46,47]

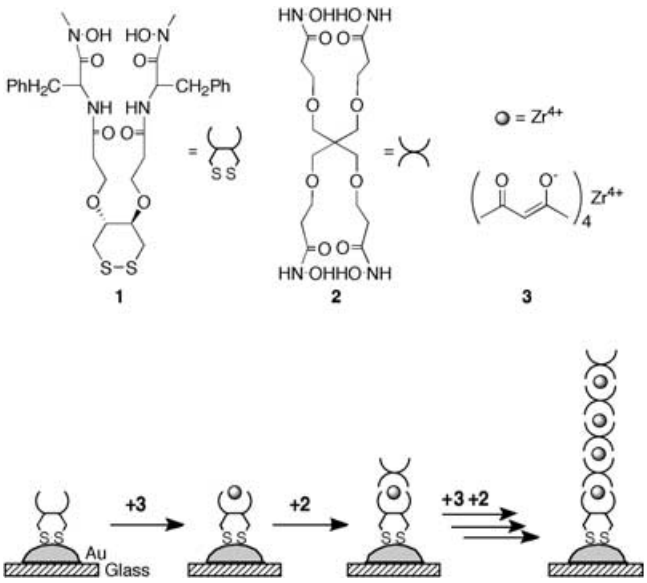

Figure 1. Building blocks and construction scheme of the coordination-based metal–organic multilayers.

The substrates used here were 1.0–5.0 nm (nominal thickness) Au island films evaporated on MPTS-modified glass (MPTS = mercaptopropyltrimethoxysilane), combining excellent adhesion of the metal to the substrate and tunable absorbance.[33] The morphology and optical properties of the multilayer-coated Au island films were studied by high-resolution scanning electron microscopy (HRSEM), atom force microscopy (AFM), X-ray photoelectron spectroscopy (XPS), and transmission UV-visible spectroscopy. A particularly slow decrease of the distance sensitivity is observed for 5.0 nm annealed Au films on silanized glass, up to 11 organic layers (ca. 15 nm from the Au surface). The superior response of these films is suitable for assembly of bulky (e.g., biological) receptors on T-SPR substrates without significant decrease in the transducer sensitivity.

Results and Discussion

Multilayer self-assembly on gold island films: Ultrathin gold films evaporated on MPTS-modified glass substrates show excellent adhesion to the substrate, favoring their use as T-

SPR-based sensors. Adjustment of the morphology and optical properties of such films can be achieved by variation of the film nominal thickness, evaporation rate, and post-deposition annealing conditions. In the present case Au island films of 1.0, 2.5, and 5.0 nm nominal thickness, unannealed and annealed (200° C for 20 h), served as substrates for the layer-by-layer assembly of metal–organic multilayers. Details on the Au island film properties are given elsewhere.[33]

Construction of coordination-based self-assembled multilayers on the Au island films generally followed our previously published methodology,[42–44] shown schematically in Figure 1. The anchor monolayer adsorbed directly on the Au islands comprised the disulfide–bishydroxamate molecule **1**, while the repeat unit was the bifunctional tetrahydroxamate ligand **2**, coordinated through Zr^{IV} ions. We have recently modified the multilayer preparation scheme, replacing $ZrCl_2$ with $Zr(acac)_4$ in the ion-binding step.[45] Multilayer construction occurs by alternate binding of Zr^{IV} and ligand **2**, resulting in the addition of a single organic layer in each step. Detailed characterization of such multilayers prepared on a continuous, 100-nm-thick gold substrate, by using ellipsometry, contact-angle measurements, and XPS, showed linear growth of a multilayer with nearly ideal 1:1 metal/ligand stoichiometry, while AFM height measurements of scratched multilayers gave a thickness increase of 1.4 ± 0.17 nm per step.[45]

Morphology of coordination-based multilayers constructed on Au island films: Multilayers were constructed on Au films of 1.0, 2.5, and 5.0 nm (nominal thickness), unannealed and annealed. T-SPR measurements showed that the 1.0 nm Au films are not sensitive enough for monitoring multilayer construction (see below), hence the morphology study was limited to the 2.5 and 5.0 nm films. Coordination multilayers on Au island films were characterized by using a combination of HRSEM and AFM. HRSEM imaging by SE (secondary electrons) provides a surface morphology contrast that is enhanced by BSE-induced (BSE = backscattered electrons) SE at the Au island location below the multilayers. The images thus appear transparent to the organic layer, enabling comparison of the Au island morphology before and after multilayer formation, while AFM provides complementary information on changes in the surface topography. The number of layers in each sample was chosen according to the sensitivity of the SP absorption to thickness increase.

HRSEM images of bare and multilayer-covered Au island films (Figure 2) are visually similar, showing the same surface density and shape of the Au islands. This indicates that

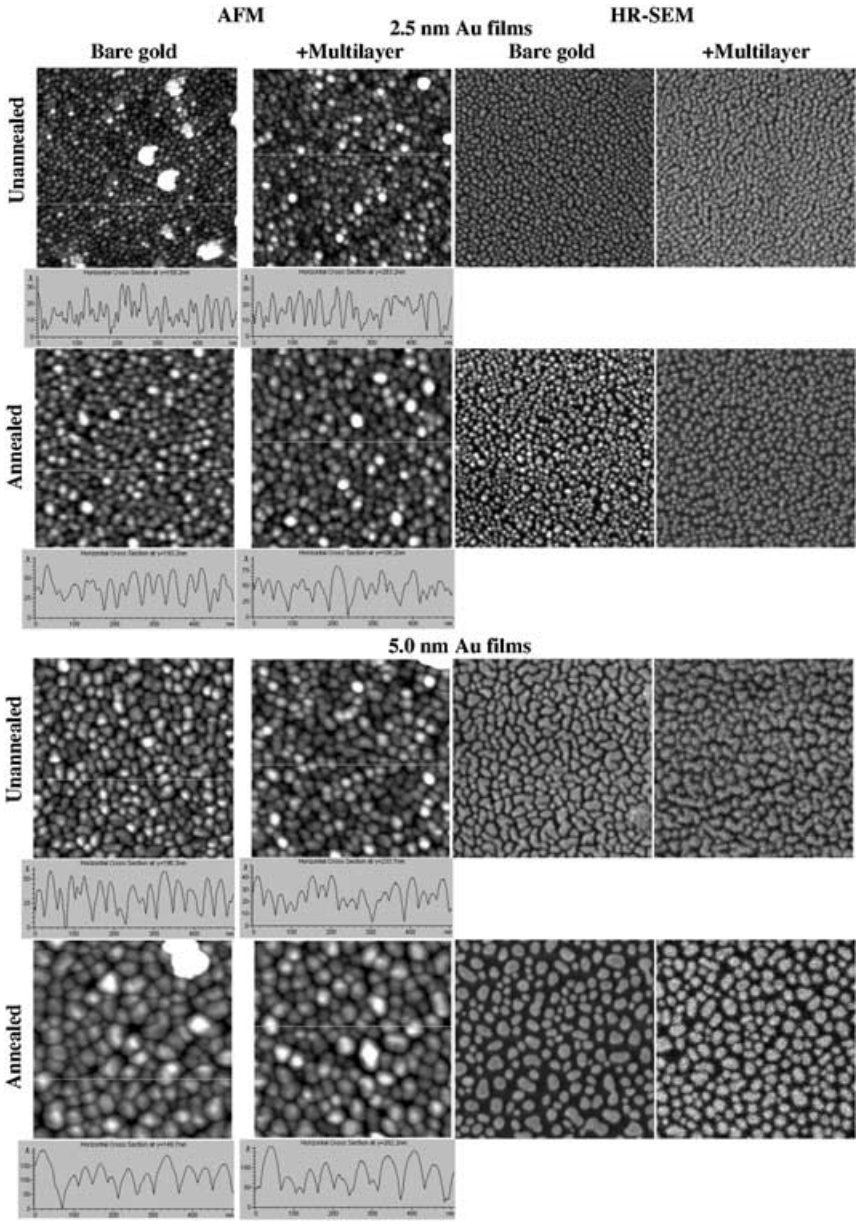

Figure 2. AAC mode AFM and HRSEM images (500×500 nm^2) of ultrathin Au island films on silanized glass before and after multilayer construction. The number of organic layers in the multilayer: 6 (2.5 nm, unannealed); 9 (5.0 nm, unannealed); 11 (2.5, 5.0 nm, annealed). A representative cross-section is shown under each AFM image.

the good adhesion of Au islands to the silanized glass prevents noticeable island shifting and reshaping during multilayer construction.[48] For example, the number of islands (counted manually) in a 200×200 nm^2 area in the 2.5 nm annealed Au films before and after multilayer construction is 114 and 116, respectively (practically the same). The decreased sharpness in the HRSEM images of multilayer-covered samples is attributed to reduced SE resolution in the images of these samples. It mainly corresponds to the SE MFP (mean free path), which is approximately 5.5 nm for carbon (at the multilayer surface) and 1 nm at bare Au island regions. The SE induced by BSE spread through the multilayer; this further contributes to delocalization of the SE signal at the multilayer surface.

AFM images of bare and multilayer-covered Au island films are also shown in Figure 2. The AAC AFM mode used here is sensitive to soft matter on the corrugated surface; that is, the tip does not penetrate the organic layer and follows the surface topography. The average AFM-derived lateral dimension of the islands in the 2.5 nm films appears larger after multilayer construction, while there is a decrease in the number of islands in the AFM images of 2.5 nm films (more pronounces in the unannealed sample) upon multilayer construction; in the 5.0 nm films the island density remains almost identical. The AFM images are influenced by the tip diameter (ca. 10 nm), which is similar to, or larger than, the average separation between islands[33] (~5–6 nm for 2.5 nm and unannealed 5.0 nm films; ~12 nm for annealed 5.0 nm films). In the case of the "rolling hills" topography typical of island films, the upper part of the grains would be imaged correctly, while the interparticle region is affected by tip convolution. In the case of the 5.0 nm films, for which the 2D AFM-imaged morphology is nearly unaffected by the multilayer (Figure 2), the change in topography is evident in the 3D images (Figure 3), in which substantial flattening is seen with sharp features disappearing in the images of the multilayer-covered island films.

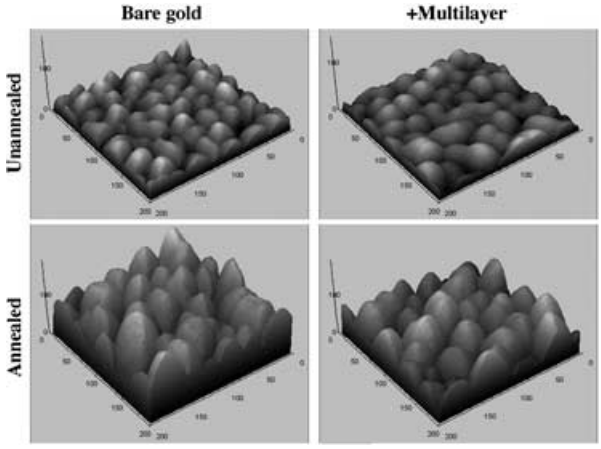

Figure 3. 3D AFM images (200×200 nm^2) of 5.0 nm unannealed and annealed Au island films before and after multilayer construction (number of organic layers as in Figure 2). z scale bar in all images is 10 nm.

The step-by-step process of multilayer construction was also evaluated by XPS. Figure 4 shows normalized atomic concentrations of C, N, and Zr versus the number of organic

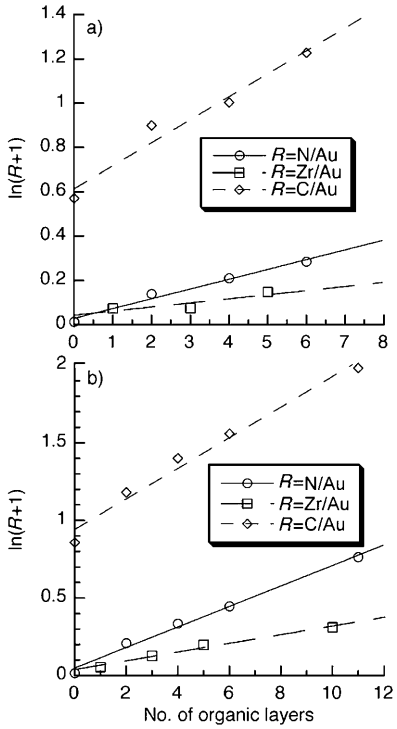

Figure 4. Atomic concentration ratios from XPS measurements vs. number of organic layers assembled on 2.5 nm unannealed (a) and annealed (b) Au island films. The lines are a linear fit to the data points.

layers assembled on unannealed and annealed 2.5 nm Au island films.[49] The linear increase in log[intensity ratio] of the overlayer elements (Zr, C, N vs. Au) with the number of organic layers indicates regular growth of the film thickness, as shown for coordination multilayers grown on a continuous, 100-nm-thick gold substrate.[43–45] It is therefore concluded that the construction of coordination multilayers on the Au island films proceeds in a regular fashion, such that the contribution of each additional organic layer to the overall film thickness is approximately the same. The thickness increment per added monolayer is assumed to be approximately 1.4 nm, as measured on continuous gold substrates (see above).[45]

Transmission spectra of gold island films: A series of transmission UV-visible spectra were measured during construction of multilayer film on 1.0, 2.5, and 5.0 nm Au films, unannealed and annealed. After each added layer the sample was rinsed and dried, and a transmission spectrum was taken in air. The spectra of 1.0 nm Au films were not sensitive enough for effectively monitoring multilayer construction, therefore the analysis below concentrates on 2.5 and 5.0 nm films. Representative spectra of 2.5 and 5.0 nm Au films are shown in Figure 5a–d. In all cases a similar devel-

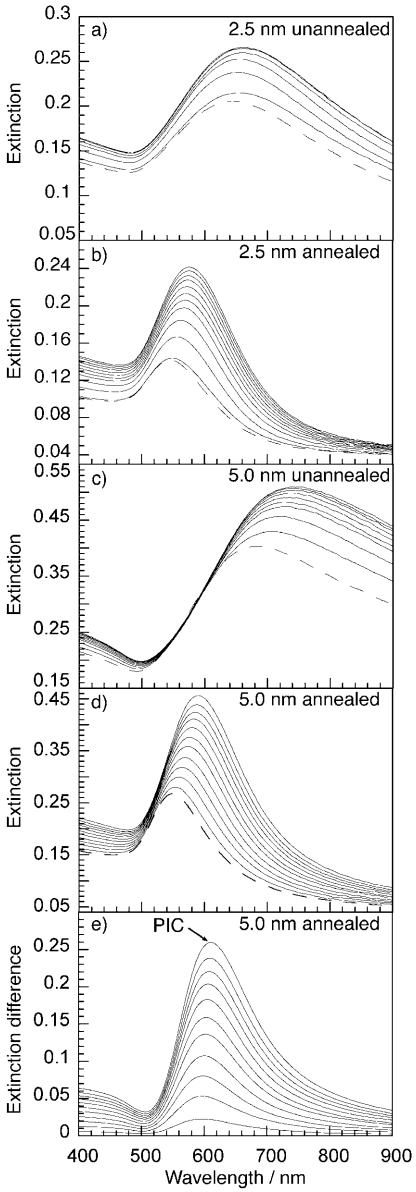

Figure 5. a)–d) Sequential transmission UV-visible (T-SPR) spectra of 2.5 and 5.0 nm gold island films (unannealed and annealed) taken after construction of each organic layer. Dashed lines correspond to the bare gold. e) Difference spectra (spectrum of the bare Au subtracted) for the construction of a coordination multilayer on 5.0 nm annealed Au film (data from Figure 5d).

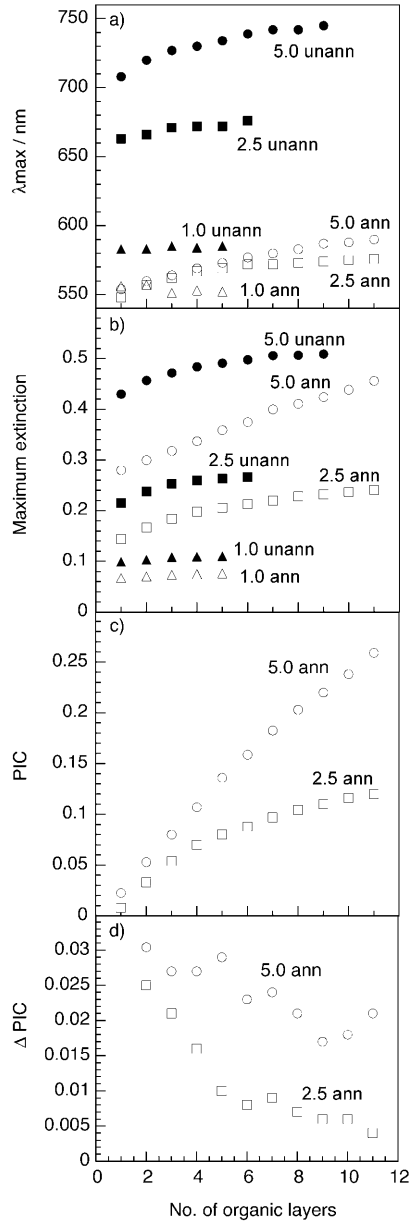

Figure 6. a) Wavelength of maximum extinction, b) maximum intensity of the SP band, and c) plasmon intensity change (PIC), of Au island films (nominal thickness indicated) during step-by-step assembly of metal–organic layers (data from Figure 5). d) The change in the PIC in each step, obtained by subtracting the PIC of each layer n from that of layer $n+1$.

opment is seen in the spectra, that is, an increase of the extinction and a red shift of the maximum of the SP band upon addition of organic layers. The system behavior qualitatively conforms to the expected response of the SP band to an increase of the effective dielectric constant near the surface of Au islands.[1,50,51] Figure 6 summarizes the changes in two characteristic parameters of the T-SPR spectra, that is, wavelength (Figure 6a) and intensity (Figure 6b) of the SP maximum absorbance, with the number of organic layers assembled on unannealed and annealed Au island films. Both parameters vary uniformly with increasing number of layers, approaching saturation at a certain thickness.

While evolution of the transmission spectra of the different films is qualitatively similar, noted differences between the films are observed upon increasing the number of layer (Figures 5a–d and 6a,b). In general, thinner Au films reach saturation of the SP band at a lower overlayer thickness. The decay in distance sensitivity obtained with the 5.0 nm annealed film is much slower than that observed with all other films. The wavelength and intensity of the SP maxi-

mum of the 5.0 nm annealed film change significantly throughout the entire measured range (11 organic layers, including the anchor layer, ca. 15 nm overall thickness; Figures 5d and 6a,b). Saturation of the SP band of this film was not reached in the present experiment. For all other substrates the change in both parameters decreases fast with increasing number of layers (Figures 5a–c and 6a,b), showing loss of distance sensitivity and saturation of the signal.

Figure 6a,b indicates that annealed Au island films show better distance sensitivity of the SP band than their unannealed counterparts. Comparison with morphology data (Figure 2) suggests that the improved sensitivity is related to the island height and/or average separation between islands, increased by annealing.[33]

Figure 5e shows the plasmon intensity change (PIC)[9,10] (obtained by subtracting the spectrum of the bare Au) for the 5.0 nm annealed Au substrate. The results, together with those of the 2.5 nm annealed Au substrate, are shown in Figure 6c,d, emphasizing the superior distance sensitivity of the thicker film.

Conclusion

The sensitivity and distance dependence of Au island films in T-SPR measurements were evaluated through layer-by-layer construction of coordination-based self-assembled multilayers. The multilayer system has been shown previously to afford regular growth on thick, continuous Au films, with a thickness increment of approximately 1.4 nm per step. The present study showed that a similar linear growth mode applies to a multilayer constructed on discontinuous Au island films. The morphology of bare and multilayer-covered Au island films evaporated on silanized glass was studied by combined HRSEM (showing the metal islands) and AFM (showing the 3D topography) images. The Au islands appear to be unaffected by the multilayer growth, while the topography shows significant flattening induced by the organic overlayer.

The layer-by-layer growth of the metal–organic overlayer on Au island films (1.0, 2.5 and 5.0 nm nominal thickness, unannealed or annealed 20 h at 200°C) was monitored at each step by T-SPR spectroscopy. The distance dependence of the SP absorbance is strongly dependent on the film preparation conditions, that is, nominal thickness and annealing. The results do not, however, provide evidence as to the influence of each structural parameter, as all the characteristic dimensions (island diameter, height, shape, separation) vary between samples.[33] The present experimental data on the distance dependence of the SP band, combined with our previous morphological characterization of the Au island films,[33] may be useful for evaluation of theoretical models.

The best distance sensitivity of the SP extinction was obtained with 5.0 nm annealed Au island films. For these films the sensitivity of the SP intensity to the addition of organic layers exhibits only slight decrease up to the tested distance from the Au substrate, corresponding to 11 organic layers (ca. 15 nm). Clearly the limit of distance sensitivity was not approached under the present optimal conditions.

The results are promising in terms of application of the technique to the design of transducers for chemical or biological sensing, usually involving receptor layers on the transducer surface. A distance sensitivity of >15 nm from the Au island surface provides ample room for binding bulky biological receptors to the island film, while maintaining reasonable sensitivity in the sensing event, that is, binding of a specific analyte to the receptor layer. We have recently demonstrated the applicability of T-SPR sensing to specific avidin recognition using a biotinylated Au island surface.[14]

While in other studies the quantity commonly measured is changes in the wavelength of the SP band maximum, we emphasize band intensity measurements as a viable alternative. Particularly attractive for sensing applications is measurement of the plasmon intensity change (PIC); that is, the maximum of the difference spectrum after subtracting the spectrum of the bare substrate (Figures 5e and 6c). As seen in Figure 5e, the position of the PIC is virtually distance independent, suggesting that this empirical observation, previously reported by us,[9,10] is quite general. Hence, PIC measurements can be carried out at a single wavelength with maximum sensitivity, thus simplifying the instrumentation and data processing.

Experimental Section

Chemicals: Molecules **1** and **2** (Figure 1) were synthesized as previously reported.[44,52] Zirconium acetylacetonate ($Zr(acac)_4$, Fluka, purum) was used without further purification. Chloroform (Biolab, AR) was passed through a column of activated basic alumina. Ethanol (Merck, AR), isopropanol (Frutarom, Analytical), H_2O_2 (30%, Frutarom), H_2SO_4 (95–98%, Palacid), 3-mercaptopropyltrimethoxysilane (MPTS, Aldrich, 97%) were used as received. Water was triply distilled. The gas used was purified house nitrogen (from liquid N_2).

Gold film preparation: Glass slides (10×18 mm^2), No. 2 (Menzel-Glaser, Germany), were immersed in freshly prepared "piranha" solution (hot 1:3 H_2O_2 30%/H_2SO_4 95–98%) for 15 min and rinsed with triply distilled water. (*Caution: Piranha solution reacts violently with organic materials and should be handled with extreme care.*) This procedure was repeated twice, after which the slides were rinsed with ethanol, dried under a nitrogen stream, and held for about 10 min at 100°C. The slides were immersed for 10 min in a mixture of MPTS (1.9 mL), water (1.4 mL), and isopropanol (100 mL), which was brought to reflux, then rinsed with isopropanol, dried under a nitrogen stream, and cured in an oven at 100–107°C for 8 min. The silanization procedure was carried out three times.[53] The silanized glass slides were mounted in a cryo-HV evaporator (Key High Vacuum) equipped with a Maxtek TM-100 thickness monitor for evaporation of the ultrathin Au films. Homogeneous Au deposition was achieved by moderate rotation of the substrate plate. Gold (99.99%, Holland-Moran, Israel) was evaporated from a tungsten boat at $2–4\times10^{-6}$ Torr at a deposition rate of 0.005–0.01 nm s^{-1}. Post-deposition annealing of Au-covered slides was carried out in air at 200°C for 20 h, by using a Ney Vulcan 3–550 oven. The heating rate was 5°C min^{-1}; the annealed slides were left to cool in air to room temperature.

Multilayer self-assembly: Prior to self-assembly the Au island substrates were stabilized in $CHCl_3$/EtOH (1:1), as previously described.[33] Monolayers of the anchor molecule **1** (Figure 1) were adsorbed from a solution

of **1** (3 mM) in $CHCl_3$/EtOH (1:1) overnight, followed by rinsing with chloroform and ethanol and immersion in ethanol for 20 min. Zr^{IV} was bound to the monolayer of **1** from a solution of $Zr(acac)_4$ (1 mM) in ethanol for 1 h, followed by rinsing and immersion in ethanol for 10 min.[45] The repeat unit **2** (Figure 1) was coordinatively bound by exposure of the surface complex to a solution of the tetrahydroxamate **2** (3 mM) in ethanol overnight, followed by ethanol rinse. The sample was then treated repeatedly with the metal ion and the organic tetrahydroxamate, resulting in a multilayer structure with a controlled number of layers.

UV-visible spectroscopy: Measurements were carried out ex situ (in air) by using a Varian CARY 50 UV/VIS/NIR spectrophotometer with a specially designed holder.[9] The scan rate was 600 nm min^{-1}, and the bandwidth of the light source in the UV-visible region was 1.0 nm. A baseline correction procedure (the spectrum of air was taken as baseline) was executed prior to each measurement session. A transmission UV-visible spectrum was recorded for each substrate after Au deposition, and samples that showed substantial deviation from the average spectrum were discarded (about 15% of the samples). All the samples were stabilized by dipping in 1:1 $CHCl_3$/EtOH (the solvents used for self-assembly of the organic layers) and drying under a stream of nitrogen.[33] The indication for stability of the Au island films was the SP extinction peak measured in air, which stopped changing after about 10 min in the solution (this time varied somewhat between samples).

Atomic force microscopy (AFM): AFM images were recorded in air by using Molecular Imaging PicoScan™ (Pico IC) instrument operated in the acoustic AC (AAC) mode. The cantilevers used were NSC12 series of ultrasharp silicon (MikroMasch, Estonia), with a resonant frequency of 100–200 kHz and an average tip radius of $\leq$10 nm.

X-ray photoelectron spectroscopy (XPS): XPS measurements were carried out with a Kratos Axis-HS XPS system, with a monochromatized $Al_{K\alpha}$ X-ray source (1486.6 eV). Elimination of beam-induced damage effects[54] was achieved by first studying the evolution of these effects and then performing the analysis on fresh spots using optimal experimental conditions.

High-resolution scanning electron microscopy (HRSEM): Images were obtained using a JSM-6700F high-resolution scanning electron microscope with a cold field emission electron source and an upper built-in SE detector. Low-energy SE signal suppression was performed to reduce the charging effect in the SE images, particularly important with the 1.0 and 2.5 nm samples.

Acknowledgements

We wish to thank the Israel Ministry of Science (Tashtiot Infrastructure Project), and the Israel Science Foundation, for financial support. We thank R. Lazar for the synthesis of molecules **1** and **2**.

[1] U. Kreibig, G. Bour, A. Hilger, M. Gartz, *Phys. Status Solidi A* **1999**, *175*, 351.
[2] D. Roy, J. Fendler, *Adv. Mater.* **2004**, *16*, 479.
[3] G. C. Papavassiliou, *Z. Phys. Chem.* **1976**, *257*, 241.
[4] F. Meriaudeau, T. R. Downey, A. Passian, A. Wig, T. L. Ferrell, *Appl. Opt.* **1998**, *37*, 8030.
[5] P. Orfanides, T. F. Buckner, M. C. Buncick, F. Meriaudeau, T. L. Ferrell, *Am. J. Phys.* **2000**, *68*, 936.
[6] T. R. Jensen, M. L. Duval, K. L. Kelly, A. A. Lazarides, G. C. Schatz, R. P. Van Duyne, *J. Phys. Chem. B* **1999**, *103*, 9846.
[7] M. Gluodenis, C. Manley, C. A. Foss, *Anal. Chem.* **1999**, *71*, 4554.
[8] G. Kalyuzhny, A. Vaskevich, G. Ashkenasy, A. Shanzer, I. Rubinstein, *J. Phys. Chem. B* **2000**, *104*, 8238.
[9] G. Kalyuzhny, M. A. Schneeweiss, A. Shanzer, A. Vaskevich, I. Rubinstein, *J. Am. Chem. Soc.* **2001**, *123*, 3177.
[10] G. Kalyuzhny, A. Vaskevich, M. A. Schneeweiss, I. Rubinstein, *Chem. Eur. J.* **2002**, *8*, 3850.
[11] M. D. Malinsky, K. L. Kelly, G. C. Schatz, R. P. Van Duyne, *J. Am. Chem. Soc.* **2001**, *123*, 1471.
[12] J. C. Riboh, A. J. Haes, A. D. McFarland, C. R. Yonzon, R. P. Van Duyne, *J. Phys. Chem. B* **2003**, *107*, 1772.
[13] E. Hutter, M. P. Pileni, *J. Phys. Chem. B* **2003**, *107*, 6497.
[14] M. Lahav, A. Vaskevich, I. Rubinstein, *Langmuir* **2004**, *20*, 7365.
[15] P. Englebienne, A. Van Hoonacker, M. Verhas, N. G. Khlebtsov, *Comb. Chem. High Throughput Screening* **2003**, *6*, 777.
[16] F. Frederix, J. M. Friedt, K. H. Choi, W. Laureyn, A. Campitelli, D. Mondelaers, G. Maes, G. Borghs, *Anal. Chem.* **2003**, *75*, 6894.
[17] L. Olofsson, T. Rindzevicius, I. Pfeiffer, M. Kall, F. Hook, *Langmuir* **2003**, *19*, 10414.
[18] A. J. Haes, R. P. Van Duyne, *J. Am. Chem. Soc.* **2002**, *124*, 10596.
[19] N. Nath, A. Chilkoti, *Anal. Chem.* **2002**, *74*, 504.
[20] P. W. Bohn, *Annu. Rev. Mater. Sci.* **1997**, *27*, 469.
[21] A. Otto, *J. Raman Spectrosc.* **1991**, *22*, 743.
[22] C. A. Murray, D. L. Allara, M. Rhinewine, *Phys. Rev. Lett.* **1981**, *46*, 57.
[23] C. A. Murray, D. L. Allara, *J. Chem. Phys.* **1982**, *76*, 1290.
[24] D. J. Walls, P. W. Bohn, *J. Phys. Chem.* **1989**, *93*, 2976.
[25] W. R. Thompson, J. E. Pemberton, *Anal. Chem.* **1994**, *66*, 3362.
[26] W. B. Lacy, J. M. Williams, L. A. Wenzler, T. P. Beebe, J. M. Harris, *Anal. Chem.* **1996**, *68*, 1003.
[27] P. J. Tarcha, J. DeSaja-Gonzalez, S. Rodriguez-Llorente, R. Aroca, *Appl. Spectrosc.* **1999**, *53*, 43.
[28] T. M. Cotton, R. A. Uphaus, D. Möbius, *J. Phys. Chem.* **1986**, *90*, 6071.
[29] G. J. Kovacs, R. O. Loutfy, P. S. Vincett, C. Jennings, R. Aroca, *Langmuir* **1986**, *2*, 689.
[30] M. Tsen, L. Sun, *Anal. Chim. Acta* **1995**, *307*, 333.
[31] Q. Ye, J. X. Fang, L. Sun, *J. Phys. Chem. B* **1997**, *101*, 8221.
[32] A. J. Haes, S. L. Zou, G. C. Schatz, R. P. Van Duyne, *J. Phys. Chem. B* **2004**, *108*, 109.
[33] I. Doron-Mor, Z. Barkay, N. Filip-Granit, A. Vaskevich, I. Rubinstein, *Chem. Mater.* **2004**, *16*, 3476.
[34] L. M. Liz-Marzan, M. Giersig, P. Mulvaney, *Langmuir* **1996**, *12*, 4329.
[35] T. Ung, L. M. Liz-Marzan, P. Mulvaney, *J. Phys. Chem. B* **2001**, *105*, 3441.
[36] T. Ung, L. M. Liz-Marzan, P. Mulvaney, *Colloids Surf. A* **2002**, *202*, 119.
[37] J. Schmitt, P. Machtle, D. Eck, H. Möhwald, C. A. Helm, *Langmuir* **1999**, *15*, 3256.
[38] S. Norrman, T. Andersson, C. G. Granqvist, O. Hunderi, *Phys. Rev. B* **1978**, *18*, 674.
[39] T. Jensen, L. Kelly, A. Lazarides, G. C. Schatz, *J. Cluster Sci.* **1999**, *10*, 295.
[40] K. L. Kelly, E. Coronado, L. L. Zhao, G. C. Schatz, *J. Phys. Chem. B* **2003**, *107*, 668.
[41] L. M. Liz-Marzan, *Mater. Today* **2004**, *7*, 26.
[42] A. Hatzor, T. van der Boom-Moav, S. Yochelis, A. Vaskevich, A. Shanzer, I. Rubinstein, *Langmuir* **2000**, *16*, 4420.
[43] I. Doron-Mor, A. Hatzor, A. Vaskevich, T. van der Boom-Moav, A. Shanzer, I. Rubinstein, H. Cohen, *Nature* **2000**, *406*, 382.
[44] A. Hatzor, T. Moav, H. Cohen, S. Matlis, J. Libman, A. Vaskevich, A. Shanzer, I. Rubinstein, *J. Am. Chem. Soc.* **1998**, *120*, 13469.
[45] I. Doron-Mor, H. Cohen, S. R. Cohen, R. Popovitz-Biro, A. Shanzer, A. Vaskevich, I. Rubinstein, *Langmuir* **2004**, *20*, 10727.
[46] A. Vaskevich, I. Doron-Mor, M. Lahav, Z. Barkay, I. Feldman, I. Rubinstein, in *Annual Meeting of the Israel Chapter of the Electrochemical Society*, Ramat-Gan, Israel, **2003**.
[47] I. Doron-Mor, H. Cohen, Z. Barkay, A. Vaskevich, I. Rubinstein, in *64th Meeting of the Israel Chemical Society*, Tel-Aviv, Israel, **2004**.
[48] We have previously shown mobility of silica islands on an untreated Au surface induced by thiol monolayer self-assembly; see: K. Shabtai, S. R. Cohen, H. Cohen, I. Rubinstein, *J. Phys. Chem. B* **2003**, *107*, 5540.

[49] The zero-layer value of the carbon corresponds to the adhesion layer and to some contamination present on the gold grains; the latter is removed in the first adsorption step.
[50] R. Doremus, *Thin Solid Films* **1998**, *326*, 205.
[51] Ellipsometric measurements performed by us on $Zr(acac)_4$–tetrahydroxamate multilayers on flat Au surfaces, combined with AFM measurement of the multilayer thickness, gave a refractive index (at 632.8 nm) of $n_f = 1.45$, $k_f = 0$. A close value ($n_f = 1.5$) was reported for Zr^{IV}–dialkylphosphonate multilayers, see: D. G. Hanken, R. M. Corn, *Anal. Chem.* **1995**, *67*, 3767.
[52] T. Moav, A. Hatzor, H. Cohen, J. Libman, I. Rubinstein, A. Shanzer, *Chem. Eur. J.* **1998**, *4*, 502.
[53] C. A. Goss, D. H. Charych, M. Majda, *Anal. Chem.* **1991**, *63*, 85.
[54] E. Frydman, H. Cohen, R. Maoz, J. Sagiv, *Langmuir* **1997**, *13*, 5089.

Received: January 28, 2005
Published online: July 11, 2005

